You, S.; Huang, Y.; Dieringa, H.; Maawad, E.; Gan, W.; kainer, K.U.; Hort, N.:
The Role of Second Phases on the Creep Behavior of As-Cast and Hot-Extruded Mg-Ca-Zr Alloys.
In: JOM: Journal of the Minerals, Metals and Materials Society. Vol. 71 (2019) 7, 2227 - 2234.
First published online by Springer: May 06, 2019

DOI: /10.1007/s11837-019-03515-7
https://dx.doi.org/10.1007/s11837-019-03515-7

The Role of Second-phases on the Creep Behavior of As-cast and Hot-extruded Mg-Ca-Zr Alloys

S. You[1,3], Y. Huang[1], H. Dieringa[1], E. Maawad[2], W. Gan[2], K.U. Kainer[1] and N. Hort[1]

1.— Institute of Materials Research, Helmholtz-Zentrum Geesthacht, Max-Planck-Straße 1, 21502 Geesthacht, Germany. 2.— German Engineering Materials Centre (GEMS), Helmholtz-Zentrum Geesthacht, Max-Planck-Straße 1, 21502 Geesthacht, Germany. 3.— E-Mail: sihang.you@hzg.de

Abstract

The effect of second phases on the creep behavior of Mg-Ca-Zr alloys was investigated. Casting and hot-extrusion processes were performed to prepare Mg-xCa-0.5Zr (x =0, 0.3 and 0.6 wt.%) alloys with different morphologies and distributions of second phases. The as-cast microstructures of Mg-Ca-Zr alloys consisted of Mg matrix and coarse Mg_2Ca intermetallic compounds distributed at grain boundaries. The hot-extruded microstructures exhibited finer Mg_2Ca spherical particles and precipitates distributed homogeneously inside the matrix and along grain boundaries. The results of creep tests suggested that the viscous glide of dislocation and dislocation climb were the dominant creep mechanisms of Mg-Ca-Zr alloys crept at 200 ℃. The creep property was strongly related to the morphology and distribution of Mg_2Ca phases. The finer and more homogeneously distributed particles showed a better strengthening effect than the coarser intermetallic compounds distributed along grain boundaries.

Introduction

Magnesium is the lightest structural metal with high specific strength, good electric conductivity as well as thermal conductivity [1,2]. However, owing to their low strength and formability at room temperature and poor creep resistance at elevated temperatures, the present applications of magnesium alloys are still limited. In recent years, great efforts have been made to develop high-creep-resistant Mg alloys. The addition of rare earth (RE) elements is generally regarded as the most effective way to improve the creep resistance of Mg alloys [3]. However, RE elements are still too expensive to be widely used in Mg alloys [4]. Among all non-RE alloying elements, Ca is expected to be an effective alloying element in the development of creep-resistant Mg alloys due to its low cost and even lower density than Mg. It has been reported that the creep resistance of most widely used Mg-Al based alloys can be enhanced by Ca addition [5,6], since Ca could consume Al solutes and introduce more thermally stable phases or precipitates [7]. Moreover, the mechanical properties and creep resistance of ternary Mg-Zn-Sn alloy was reported to be significantly improved by 1.0 wt.% of Ca addition [8]. The addition of Ca also results in refined grains [9], an enhanced ignition point [10] and a weakened texture which leads to the improvement of ductility for Mg alloys [11].

In Mg-Ca based alloys, Mg_2Ca phases play an important role in enhancing the creep properties, as aforementioned, it is a thermally stable compound with a high melting point [12] and can effectively hinder the grain boundary sliding and dislocation motion even at elevated temperatures [13]. Despite the reported literature regarding the creep behavior of many Ca-containing Mg alloy systems have been reported in recent years, the role of the distribution and morphology of second-phases on the creep behavior of binary Mg-Ca alloys was rarely investigated. The present work aims to investigate the creep behavior of Mg-Ca alloys with different Ca contents and to clarify the relationship between the creep resistance and the distribution and morphology of second phases for the alloys. Casting and hot extrusion processes were used to prepare the alloys with different distributions of second phases. A small amount of Zr was added as the grain refiner for the alloys. As-cast and hot-extruded Mg-0.5Zr alloys were prepared to be used as benchmarks.

Experimental procedures

Three alloys with different Ca concentrations (wt.%), Mg-0.5Zr, Mg-0.3Ca-0.5Zr and Mg-0.6Ca-0.5Zr alloys, were prepared by permanent mould direct chill casting [14]. Pure Mg was melted in a mild steel crucible under a protective atmosphere (Ar +2 vol.% SF6). Pure Ca and Mg-33.3wt.% Zr master alloy were then added into the melt at 750 °C. The melt was then homogenized by mechanical stirring under 200 rpm for 20 min. After that, the melt was poured into a steel crucible preheated to 680 °C and held at 680 °C for 20 min with gas protection. Finally, the melt was solidified by lowering the crucible into cooling water with a rate of 10 mm/s. The ingots for hot extrusion were first solid solution heat-treated (T4) at 500 ℃ for 8 h followed by water quenching. These T4 treated ingots were then machined to a cylinder with a size Φ49 × 150 mm and preheated at 400 ℃ for 1 h. The indirect extrusion process was carried out at 400 ℃ with a ram speed of 2 mm/s and an extrusion ratio of 25 : 1 to produce round profiles with a diameter of 10 mm.

The specimens for optical microscope (OM) observations were ground with silicon carbide abrasive paper, polished with water-free colloidal silica (OPS) and then etched with acetic-picric solution. OM observations were performed with a Leica DMI5000 microscope with a digital camera attached. The average grain size was measured by the linear intercept method from the micrographs. Microstructures were investigated using a TESCAN Vega SB-U III scanning electron microscope (SEM) under an accelerating voltage of 15 kV and working distance of 15 mm in backscatter electron (BSE) mode. The volume fraction of the intermetallic phases was determined by SEM BSE image analysis using ImageJ software. The threshold and contrast were adjusted to obtain a high contrast between the intermetallic phase regions and the matrix. At least 10 micrographs were used to determine the amount of these phases. Specimens for transmission electron microscope (TEM) were firstly ground mechanically to a thickness of about 120 μm and then thinned by electropolishing in a twin jet electropolisher using a polishing solution of 2.5 % $HClO_4$ and 97.5% ethanol at -45 ℃ and a voltage of 40 V. The TEM examinations were carried out on a Philips CM200 instrument operating at 200 kV. The bright-field mode was used for imaging the microstructure. The diffraction patterns of intermetallic particles were obtained through selected area electron diffraction (SAED). The synchrotron radiation diffraction was also used for the phase analysis, which was carried out at the high-energy X-ray beamline HEMS P07B of PETRA III, DESY (Deutsches Elektronen-Synchrotron). A monochromatic beam was used with a wavelength of 0.014235 nm and a beam cross-section of 0.7 × 0.7 mm^2. The acquisition time of each diffraction pattern was set to 0.5 s. The diffraction patterns (Debye-Scherrer rings) were recorded by a detector with an effective pixel size of 200 μm, placed 1950 mm behind the sample, calibrated by a LaB_6 standard powder sample. The diffraction patterns were integrated and analyzed with the software Fit2D. Cylindrical specimens of 15 mm in length and 6 mm in diameter were used for the compression creep tests. The constant stress compression creep tests were performed on both the as-cast and hot-extruded Mg-xCa-0.5Zr alloys at 200 ℃ under a range of stresses using Applied Test System (ATS) creep machines.

Results

The as-cast and hot-extruded optical microstructures of investigated alloys are shown in Fig. 1. Due to the addition of Zr, relatively homogeneous microstructure was formed during the direct chill casting, even though the cooling process was fast with water quenching. The grain sizes of as-cast alloys were measured as 221 ± 101 μm for Mg-0.5Zr, 79 ± 39 μm for Mg-0.3Ca-0.5Zr and 69 ± 36 μm for Mg-0.6Ca-0.5Zr alloy, respectively. The grain sizes of hot-extruded alloys containing 0, 0.3 and 0.6 wt.% Ca were measured to be 33.7 ± 15.3 μm, 15.5 ± 7.1 μm and 8.3 ± 3.5 μm, respectively. The grains of both the as-cast and extruded alloys are significantly refined with increasing Ca content.

Fig. 2 presents the SEM (BSE) microstructures of as-cast and hot-extruded alloys. The as-cast microstructures of Ca-containing alloys are mainly composed of α-Mg matrix and intermetallic phases distributed at grain boundaries. The volume fraction of these intermetallic compounds increases remarkably with increasing Ca content. It is 0.81 ± 0.11 % for as-cast Mg-0.3Ca-0.5Zr and 2.05 ± 0.30 % for Mg-0.6Ca-0.5Zr. The morphology of these compounds in the as-cast Mg-0.6Ca-0.5Zr alloy is more continuous than that in the alloy with 0.3 wt.%

Ca. For the hot-extruded alloys, the amount of intermetallic particles increases noticeably with increasing the addition of Ca. The volume fractions of intermetallic particles in hot-extruded Mg-0.3Ca-0.5Zr and Mg-0.6Ca-0.5Zr are 0.41 ± 0.08 % and 1.47 ± 0.15 %, respectively. However, the morphology and distribution of these particles are significantly different from that in the as-cast alloys. It can be observed the bright particles distribute homogeneously inside grains and along grain boundaries.

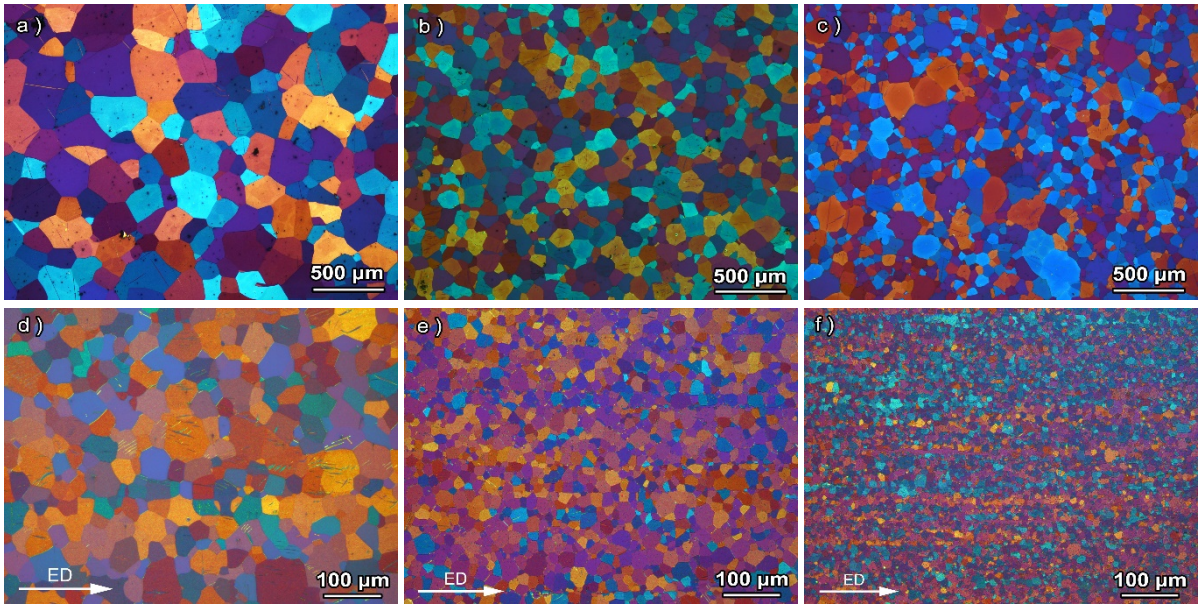

Fig. 1. Optical micrographs of as-cast (a) Mg-0.5Zr, (b) Mg-0.3Ca-0.5Zr, (c) Mg-0.6Ca-0.5Zr alloys and hot-extruded (d) Mg-0.5Zr, (e) Mg-0.3Ca-0.5Zr, (f) Mg-0.6Ca-0.5Zr alloys parallel to extrusion direction (ED).

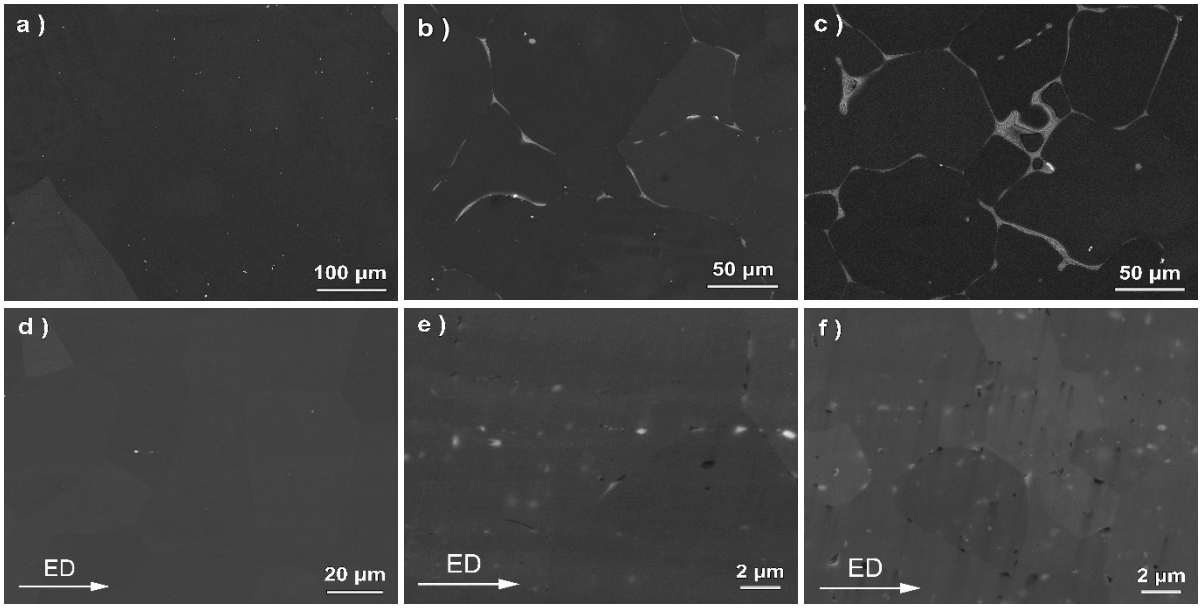

Fig. 2. SEM micrographs of as-cast (a) Mg-0.5Zr, (b) Mg-0.3Ca-0.5Zr, (c) Mg-0.6Ca-0.5Zr and hot-extruded (d) Mg-0.5Zr, (e) Mg-0.3Ca-0.5Zr, (f) Mg-0.6Ca-0.5Zr alloys.

The synchrotron diffraction line profiles of as-cast and hot-extruded alloys are shown in Fig. 3 (a) and (b), respectively. Only the peaks of α-Mg are found in the line profile of as-cast and hot-extruded Mg-0.5Zr alloy. With 0.3 wt.% Ca addition, some additional peaks of Mg_2Ca phase with relatively low intensity appear besides Mg peaks. The intensity of Mg_2Ca peaks increases significantly with increasing Ca content to 0.6 wt.% in both the as-cast and hot-extruded alloys. This indicates that both of the intermetallic compounds in the as-cast

microstructures and the spherical intermetallic particles in the hot-extruded microstructures are Mg_2Ca phases. The amount of these intermetallic phases increase with increasing Ca content, which is consistent with the SEM results shown in Fig. 2.

In hot-extruded Mg-Ca-Zr alloys, apart from those spherical particles found by SEM observations, a few fine precipitates in the matrix in nanometer order were also detected by TEM observations (Fig. 4). These small precipitates have a disc shape in the $[1\bar{2}10]$ direction, showing that they lie on basal plane of the α-Mg matrix. The EDS analysis of precipitates 1 and 2 indicate that they are Ca-enriched. In this work, due to the low content of Ca and low number density of these precipitates, it is hard to get their diffraction patterns by SAED. In Mg-Ca binary alloys, Mg_2Ca phase was recognized as the only second phase in the Mg-rich region. This second phase was confirmed in the present as-cast material. According to the observations from references [15-17], these small disc precipitates could be considered as Mg_2Ca precipitates. Further investigations will be needed to identify them in the future using the HAADF techniques.

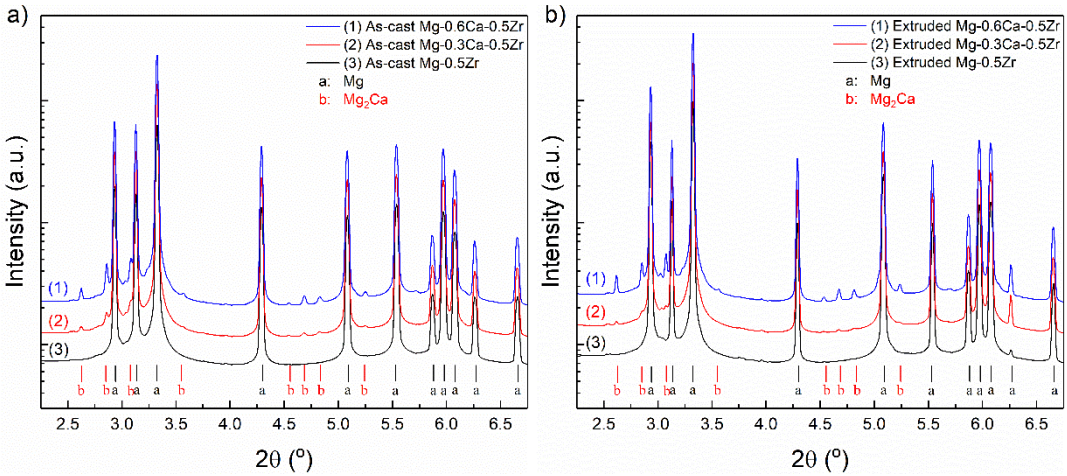

Fig. 3. Synchrotron diffraction line profiles of (a) as-cast and (b) hot-extruded Mg-Ca-Zr alloys.

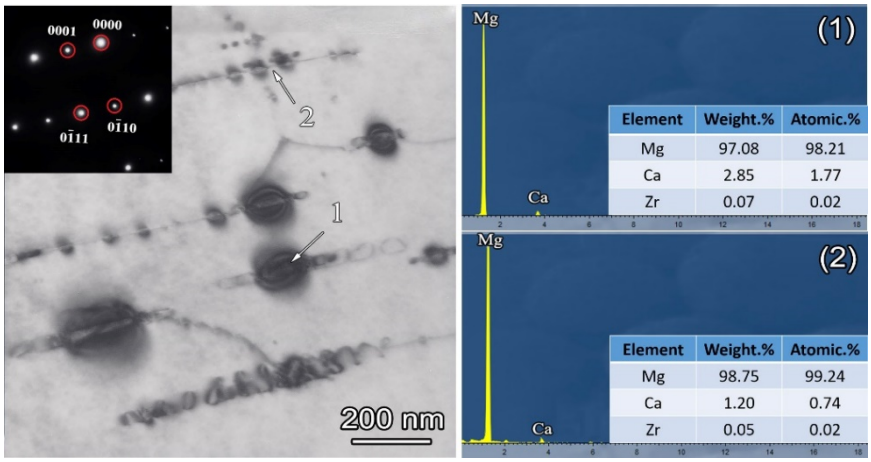

Fig. 4. Bright-field TEM images of extruded Mg-0.3Ca-0.5Zr alloy taken from $[1\bar{2}10]$ and the corresponding SAED pattern. The EDS analysis of position 1 and 2 are presented in the right figure (1) and (2).

Fig. 5 (a) and (b) present the creep strain curves of as-cast and hot-extruded alloys, respectively, at 200 °C and 40 MPa. It is found that increasing the Ca content from 0 to 0.6 wt.% improves both the primary and steady-state creep properties of as-cast alloys. However, a different situation is observed for the hot-extruded Mg-Ca-Zr alloys. The creep property is first significantly enhanced by 0.3 wt.% Ca addition, but then worsened by further Ca addition to 0.6 wt.%.

The double logarithmic plots of the minimum creep rate vs. stress with stress exponent n values for the as-cast and hot-extruded Mg-Ca-Zr alloys were presented in Fig. 6 (a) and (b), respectively. In order to compare the creep behaviors of alloys with different Ca contents, all the samples were tested with the same parameters. It can be found that the minimum creep rates of as-cast Mg-0.5Zr alloy at all stress levels reduce by around 1 order of magnitude with 0.3 wt.% Ca addition. With further addition of Ca, the minimum creep rate only slightly decreases. In contrast, for the extruded alloys, the minimum creep rate of extruded Mg-0.3Ca-0.5Zr alloy is approximately 2 orders of magnitude lower than that of extruded Mg-0.5Zr alloy. With further Ca addition, the minimum creep rate of extruded alloy continues increasing by 1 order of magnitude.

Under steady state creep condition, the steady-state creep rate $\dot{\varepsilon}_s$ can be described as a function of stress σ and temperature T at elevated temperatures [18]:

$$\dot{\varepsilon}_s = A\sigma^n exp(-Q/RT) \qquad \text{Equation (1)}$$

where A is a dimensionless material constant, n is the stress exponent, Q is the activation energy for creep and R is the gas constant. At a given temperature, most of the creep deformations of polycrystalline alloys follow a power-law relation:

$$\dot{\varepsilon}_s = k\sigma^n \qquad \text{Equation (2)}$$

where k is a constant. The stress exponent n can be evaluated by calculating the slope of the $log\dot{\varepsilon}$ versus $log\sigma$ plots at a given temperature. This n value is commonly used to infer the dominant creep mechanism for Mg alloys in specific ranges of stresses at a constant temperature [19]. Nevertheless, for the high temperature creep deformation of the alloys with second-phase particles or precipitates, it is necessary to consider the presence of threshold stress σ_t [20]. The threshold stress σ_t is defined as the limiting stress below which no measureable creep rate can be achieved and is related to the interactions between dislocations and precipitates or particles [21]. When considering the threshold stress, the steady-state creep rate $\dot{\varepsilon}_s$ can be expressed by the form:

$$\dot{\varepsilon}_s = k(\sigma - \sigma_t)^{n_t} \qquad \text{Equation (3)}$$

In this case, the true stress exponent n_t can be calculated by linear fitting the double logarithm of minimum creep rate $\dot{\varepsilon}_s$ and the effective stress $\sigma - \sigma_t$. The threshold stress of as-cast Mg-0.5Zr, Mg-0.3Ca-0.5Zr and Mg-0.6Ca-0.5Zr were calculated to be 7, 14 and 16 MPa. For the extruded alloys containing 0, 0.3 and 0.6 wt.% Ca, the threshold stresses were determined to be 4, 10 and 5 MPa. By plotting the double logarithmic plots of the minimum creep rates vs. effective stresses as shown in Fig. 6 (c) and (d), the true stress exponent n_t values at 200 ℃ for the as-cast and hot-extruded Mg-0.5Zr, Mg-0.3Ca-0.5Zr and Mg-0.6Ca-0.5Zr alloys are determined to be in the range of 3 ~ 5.

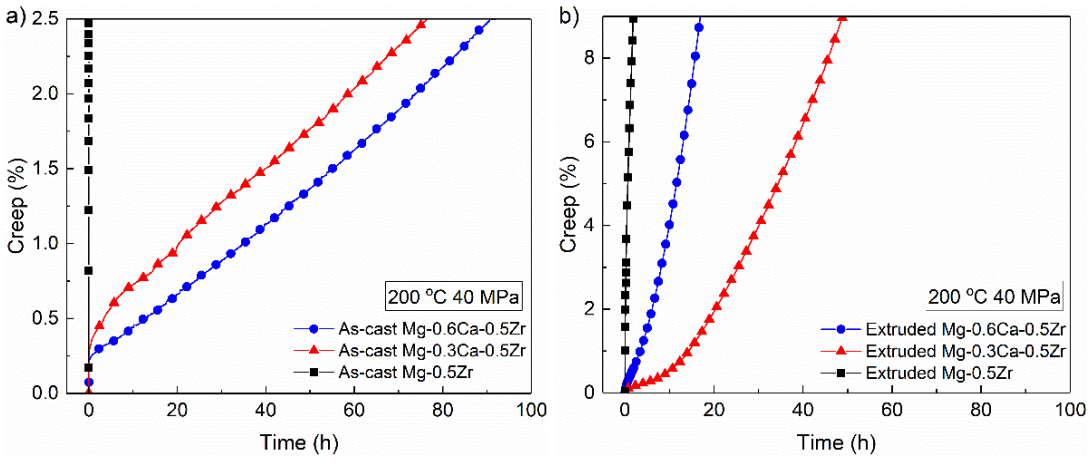

Fig. 5. Creep strain curves for (a) as-cast and (b) hot-extruded Mg-Ca-Zr alloys tested at 200 ℃, 40 MPa.

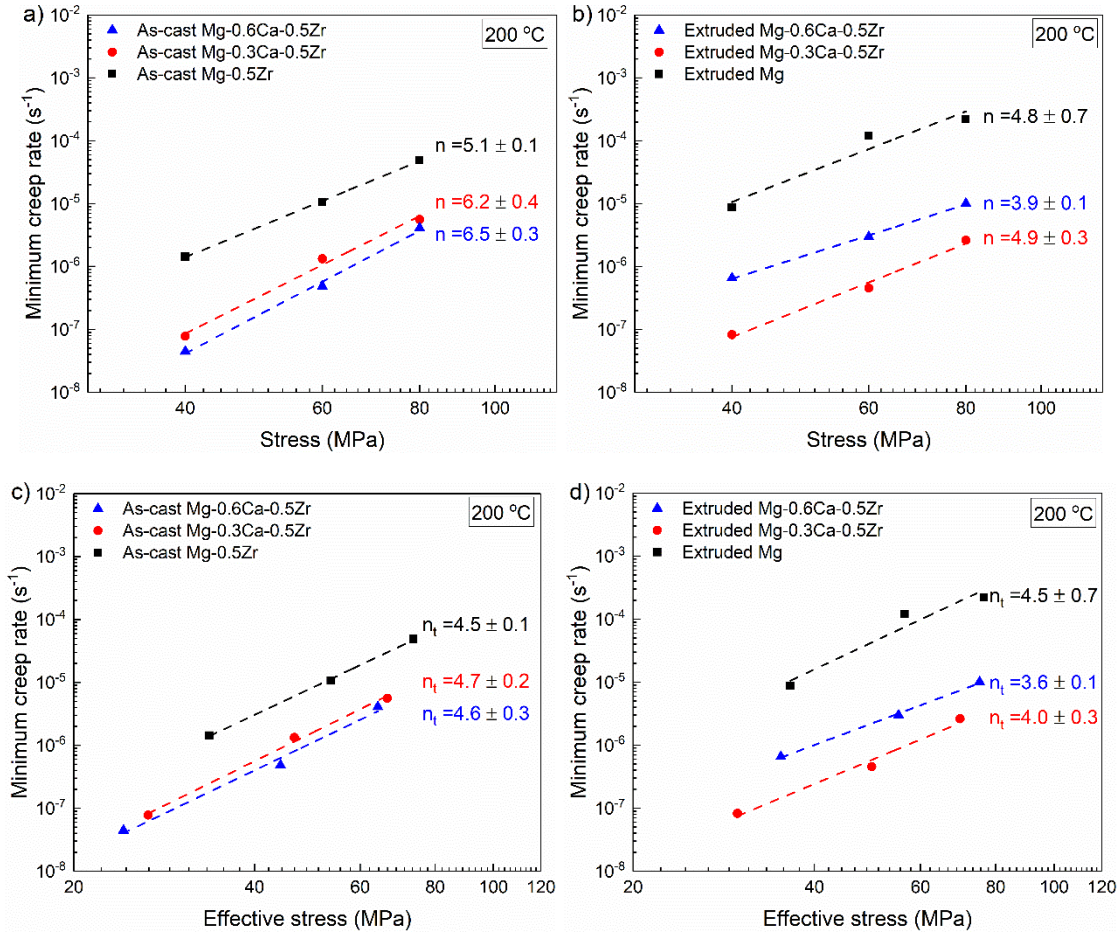

Fig. 6. Comparison of the minimum creep rates between (a) as-cast and (b) hot-extruded alloys at 200 ℃, and the minimum creep rate vs. effective stress with true stress exponents (n_t) for (c) as-cast and (d) hot-extruded alloys at 200 ℃.

Discussion

In this work, Zr was added into the alloys as a grain refiner. Its powerful grain refinement effect is due to its good crystallographic matching with Mg and its high growth restriction [22]. Since the content of present Zr addition was relatively low, most of Zr were dissolved into Mg matrix. These dissolved Zr with a high growth restriction factor allows the rapid building up of an effective constitutional supercooling zone ahead of the growing crystal, resulting in a significant grain refinement [22]. Consequently, the grain structure of all the as-cast alloys are relatively homogeneous and the grains are not very coarse after the addition of Zr. It is found that the microstructures of Ca-containing and Ca-free alloys are extremely different at both the as-cast and hot-extruded conditions. For the as-cast alloys, due to the high cooling rate associated with direct chill casting, the solidification process proceeds under a non-equilibrium condition. The distribution of Ca tends to be inhomogeneous after solidification. Since the solid solubility of Ca is low in Mg (max. 0.7 wt.% at 516.5 ℃ [23]), most of Ca atoms are contributed to the formation of Mg_2Ca phases at dendritic and grain boundaries.

For the hot-extruded alloys, T4 heat-treatment at 500 ℃ and preheating treatment at 400 ℃ were performed before the final extrusion. The Mg_2Ca compounds in the as-cast alloys are expected to be fully dissolved into the matrix during T4 heat-treatment, since the maximum solid solubility of Ca in Mg at 500 ℃ is approximate 0.65 wt.%, which is higher than the Ca content contained in the current experimental alloys. The solid solubility of Ca at 400 ℃ decrease to lower than 0.3 wt.%. As a result, Ca solutes tended to precipitate and grow as Mg_2Ca particles shown in the SEM BSE micrographs in Fig. 2 (e) and (f) during the preheating treatment. Furthermore, plastic deformation could generate a large amount of dislocations. The stress field around these dislocations could provide the driving force for mass transfer [24] and the dislocations can serve as nucleation points for precipitation. It should be noted that the formation of precipitates is related to the dislocation density. In the current work, the

extrusion temperature is 400 ℃, at which the internal stress could be released and the dislocations tended to be dynamically recovered. Thus, the dislocation density could be decreased significantly and the formation of precipitates could be restricted during hot-extrusion. As shown in Fig. 4, only a small number of fine Mg_2Ca precipitates was found in the matrix.

Compared to the hot-extruded Ca-free alloys, Ca-containing alloys exhibit finer grain microstructure. Similar results can also be found in the previous studies on Ca-containing alloys [25-27]. It was suggested that the grain refinement effect of Ca for extruded Mg alloys is most likely a consequence of the influence of Ca on the dynamic recrystallization [28]. The precipitates formed during preheating and hot-extrusion play an important role in refining grains of hot-extruded Ca containing alloys. As shown in Fig. 2(e), (f) and Fig. 4, the Mg_2Ca precipitates are distributed along grain boundaries and among matrix, which could pin the grain boundary movement and prevent the grain growth during hot-extrusion.

Regarding the creep behavior of as-cast alloys, there exist two competitive effects on the creep properties with increasing Ca content. First, the decreased grain size caused by Ca addition would worsen the creep resistance [29]. It is well known that, with increasing temperature, the grain boundaries become weak regions and creep deformations can easily occur by grain sliding. Finer grains mean a higher density of grain boundary, in other words, a higher amount of weak regions. Therefore, creep could proceed more easily in the alloys with finer grains. Second, the thermally stable Mg_2Ca particles formed along the dendritic and grain boundaries could effectively enhance the creep resistance by their pinning effects on the grain boundary sliding. In the as-cast alloys, the grain size did not change largely with the addition of Ca. Apparently, the strengthening of Mg_2Ca particles plays a more dominant role than the weakening of refined grains in influencing the creep deformation. As a result, the creep properties of as-cast alloys are improved by Ca addition. As to the extruded alloys, apart from the influence of grain size on creep properties, the homogeneously distributed Mg_2Ca precipitates are expected to effectively enhance the creep resistance by blocking the dislocations motion as well as the grain boundary sliding. Due to the extremely reduced grain size caused by 0.6 wt.% Ca addition (Fig. 1(f)), the weakening effect of a higher density of grain boundaries on the creep resistance plays a more important role than the strengthening effect of Mg_2Ca precipitates, even though the hot-extruded Mg-0.6Ca-0.5Zr has a relatively higher density of Mg_2Ca precipitates. Thus, unlike the as-cast alloy with 0.6 wt.% Ca, the extruded alloy with 0.6 wt.% Ca shows a lower creep resistance than that with 0.3 wt.% Ca. As aforementioned, the addition of 0.3 wt.% Ca shows an excellent strengthening effect on the creep resistance of alloys in both the as-cast and hot-extruded conditions. But compared with the as-cast alloy, the addition of 0.3 wt.% Ca to the extruded alloy results in a better improvement in creep resistance. The much more enhancement of creep properties caused by 0.3 wt.% Ca addition in the hot-extruded alloys may attribute to the different morphology and distribution of second phase particles in its microstructure compared to that in the as-cast alloys.

As shown in Fig. 6 (c) and (d), the true stress exponent n_t values of the as-cast and extruded Mg-Ca-Zr alloys are around 3 ~ 5 between 40 ~ 80 MPa at 200 ℃, indicating that the viscous glide of dislocation and dislocation climbing are the dominant rate-controlling deformation mechanisms during the creep deformation at 200 ℃. Based on this main creep mechanism, the more significantly improved creep properties for the extruded alloys could be explained as follows: In the as-cast alloys, although the coarse Mg_2Ca compounds distributed along grain boundaries could effectively block grain boundary sliding at elevated temperatures, their impeding effects on the dislocation motions are too limited. In contrast, in the extruded alloys, the homogeneously distributed Mg_2Ca spherical particles as well as the precipitates lied in the matrix could not only pin the grain boundaries sliding, but also serve as effective obstacles to hinder the dislocation motions. As a result, the addition of Ca shows a more significant effect on enhancing the creep properties for the extruded alloys. It could be concluded that the effects of Ca on the creep properties of Mg-Ca-Zr alloys are strongly related to the morphology and distribution of second phase particles. The finer and more homogeneously distributed Mg_2Ca particles have a greater effect on improving the creep resistance than those coarser Mg_2Ca particles distributed along grain boundaries.

Conclusions

The effects of the morphology and distribution of second phases on the creep behavior of as-cast and hot-extruded Mg-Ca-Zr alloys were investigated. The following conclusions can be drawn:

- The as-cast microstructures of Mg-Ca-Zr alloys consist of α-Mg and coarse Mg_2Ca compounds distributed along dendritic and grain boundaries, while the hot-extruded microstructures are composed of Mg_2Ca precipitates and spherical particles homogeneously distributed in the matrix and along grain boundaries.
- The creep resistance of both the as-cast and hot-extruded Mg-Ca-Zr alloys can be improved by 0.3 wt.% Ca addition. With further addition of Ca more than 0.3 wt.%, the creep property of extruded alloys is worsened due to the extremely reduced grain size.
- The effect of Ca on the creep properties of Mg-Ca alloys is strongly related to the morphology and distribution of Mg_2Ca phases. The finer and more homogeneously distributed Mg_2Ca particles have a greater effect on improving the creep properties.

Acknowledgements

The authors are thankful to Mr. G. Meister from MagIC at Helmholtz-Zentrum Geesthacht for technical supports. One of the authors (S. You) acknowledges the financial support from China Scholarship Council (CSC).

References

1 K.U. Kainer, *Magnesium Alloys and Technology,* 1st ed. (Germany: John Wiley & Sons, 2003), pp. 1-3.
2 A.A. Luo, *J. Magnesium Alloys,* 1, 2 (2013).
3 B. Mordike, *Mater. Sci. Eng., A,* 324, 103 (2002).
4 N. Mo, Q. Tan, B. Jiang, F. Pan & M.-X. Zhang, *Metall. Mater. Trans. A,* 48, 5710 (2017).
5 J. TerBush, A. Suzuki, N. Saddock, J. Jones & T. Pollock, *Scr. Mater.,* 58, 914 (2008).
6 S. Xu, N. Matsumoto, K. Yamamoto, S. Kamado, T. Honma & Y. Kojima, *Mater. Sci. Eng., A,* 509, 105 (2009).
7 B. Kondori & R. Mahmudi, *Mater. Sci. Eng., A,* 700, 438 (2017).
8 M. Yang, L. Cheng, J. Shen & F. Pan, *Rare Met.,* 28, 576 (2009).
9 D.H. StJohn, M. Qian, M.A. Easton, P. Cao & Z. Hildebrand, *Metall. Mater. Trans. A,* 36, 1669 (2005).
10 J. Fan, G. Yang, Y. Zhou, Y. Wei & B. Xu, *Metall. Mater. Trans. A,* 40, 2184 (2009).
11 N. Zhou, Z.Y. Zhang, J. Dong, L. Jin & W.J. Ding, *Mater. Sci. Eng., A,* 560, 103 (2013).
12 K. Ozturk, Y. Zhong, A.A. Luo & Z.K. Liu, *Jom-J Min Met Mat S,* 55, A40 (2003).
13 Y. Terada, D. Itoh & T. Sato, *Mater. Sci. Eng., A,* 523, 214 (2009).
14 F.R. Elsayed, N. Hort, M.A. Salgado Ordorica & K.U. Kainer, *Mater. Sci. Forum,* 690, 65 (2011).
15 J.C. Oh, T. Ohkubo, T. Mukai & K. Hono, *Scr. Mater.,* 53, 675 (2005).
16 K. Oh-ishi, R. Watanabe, C.L. Mendis & K. Hono, *Mater. Sci. Eng., A,* 526, 177 (2009).
17 H. Pan, G. Qin, Y. Ren, L. Wang, S. Sun & X. Meng, *J. Alloys Compd.,* 630, 272 (2015).
18 K.R. Athul, U.T.S. Pillai, A. Srinivasan & B.C. Pai, *Adv. Eng. Mater.,* 18, 770 (2016).
19 H. Somekawa, K. Hirai, H. Watanabe, Y. Takigawa & K. Higashi, *Mater. Sci. Eng., A,* 407, 53 (2005).
20 Y. Li & T.G. Langdon, *Scr. Mater.,* 36, 1457 (1997).
21 J. Gibeling & W. Nix, *Mater. Sci. Eng.,* 45, 123 (1980).
22 D.H. StJohn, M.A. Easton, M. Qian & J.A. Taylor, *Metall. Mater. Trans. A,* 44, 2935 (2013).
23 M. Aljarrah & M. Medraj, *CALPHAD,* 32, 240 (2008).
24 D. Blavette, E. Cadel, A. Fraczkiewicz & A. Menand, *Science,* 286, 2317 (1999).
25 J. Oh, T. Ohkubo, T. Mukai & K. Hono, *Scr. Mater.,* 53, 675 (2005).
26 Y. Ortega, M.A. Monge & R. Pareja, *J. Alloys Compd.,* 463, 62 (2008).
27 L. Geng, B. Zhang, A. Li & C. Dong, *Mater. Lett.,* 63, 557 (2009).
28 B. Zhang, Y. Wang, L. Geng & C. Lu, *Mater. Sci. Eng., A,* 539, 56 (2012).
29 R. Coble, *J. Appl. Phys.,* 34, 1679 (1963).